Available online at www.sciencedirect.com
SCIENCE DIRECT
Thermochimica Acta 446 (2006) 73–83
thermochimica acta
www.elsevier.com/locate/tca

High pressure–low temperature calorimetry I. Application to the phase change of mercury under pressure

F. Dan [a], J.-P.E. Grolier [b,*]

[a] *Department of Macromolecular Chemistry, Gh.Asachi Technical University, 71 Mangeron Ave., 700050 Iasi, Romania*
[b] *Laboratory of Thermodynamics of Solutions and Polymers, University Blaise Pascal, 24 des Landais Ave., 63177 Aubière, France*

Abstract

The melting and crystallization behaviour of pure mercury under pressure was experimentally investigated using a scanning calorimeter, which is a sensitive Calvet type differential calorimeter combined with a computer controlled high-pressure pump driven by a stepping motor. In order to have a good control of calorimetric block temperature, starting from −75 °C, the jacket of calorimetric block was connected to a powerful cryostat, which is also computer controlled. This set-up allows to determine the latent heat of fusion/crystallization of mercury and the associated volume changes. Typically, one of the independent variable (*p*, *V*, or *T*) is kept constant, another one is changed with time, and both the enthalpy effect and the change of the remaining third variable are measured with high accuracy. Fusion/crystallization of mercury was investigated both during temperature and pressure scans and *n*-propanol was used as pressurization fluid. Both methods gave high accuracy data of latent heat of fusion/crystallization of pure mercury. The data obtained by the two different methods are comparatively discussed and making use of Clapeyron equation, the pressure and temperature derivatives of the mercury melting temperature were calculated. A special attention was paid to the manner in which the pressurization rate affects the calorimetric signal.

Keywords: Scanning transitiometry; Low temperature; High pressure; Mercury; Phase change

1. Introduction

Calorimetric methods have always been widely used in investigation of phase transitions. Phase transitions are very important in industrial practice; ignorance of a phase diagram, particularly at extreme conditions of pressure, temperature, and of chemical reactivity, is a limiting factor to the development of industrial processes [1].

When the goal is to investigate the pressure effects on the physical properties of compounds the calorimetric set-up must be adapted by adding an high-pressure line; it requires pressure resistant and heavy cells and, at least, two problems which are not easy to handle must be solved, namely: high pressure, up to 500 MPa, and need of special equipment with skillful experience in their use [2]. There are few currently available commercial high-pressure calorimeters, so that potential workers in this field must construct their own. However, introducing pressure as an additional variable in thermal analysis gives additional insight into the behaviour of investigated systems and a better understanding of their thermodynamics. Calorimeters operating with a single cell and with two cells (*viz.*, differential), respectively, were used in this aim and a detailed comparison concerning the measure of the latent heat of fusion of water was reported [3]. In the case of single cell calorimeters, the heat dissipated by the cell has to be subtracted from the overall calorimetric signal [4]. With the two cell calorimeters the heat flux detectors are mounted into so-called *twin differential* arrangement. Two systems – measuring and reference – are made as equal as possible to one another and they operate in common surrounding in a symmetric arrangement. If the measuring errors in both systems are nearly equal, they can be offset by differential measurements and all external perturbations are compensated.

Another problem to face concerns the pressure-transmitting medium, which necessarily enters the cells. Two different principles have been used, namely, constant mass or constant volume. Most of the studies available in literature related to liquids used the constant volume technique. The studied liquid was itself the pressure-transmitting fluid. The constant mass approach can instead be used for solid materials. It was presented by some

* Corresponding author. Tel.: +33 473 407186; fax: +33 473 407185.
E-mail address: J-Pierre.Grolier@univ-bpclermont.fr (J.-P.E. Grolier).

0040-6031/$ – see front matter © 2006 Elsevier B.V. All rights reserved.
doi:10.1016/j.tca.2006.05.014

authors [5,6]; one device [5] used mercury as a pressurization fluid and the sample to be studied was installed above the mercury level (the sample was then 'floating' above the mercury, beneath the obturator of the cell) or the sample was placed either into an open glass ampoule or enclosed in a flexible, lead or plastic, pouch. When the aim is to investigate in interactions between the solid samples and supercritical fluids, the last ones act as pressure-transmitting fluids [1,7–9].

In most applications high-pressure calorimetry is carried out at constant pressure while the tracked phenomenon is observed on increasing or decreasing the temperature (either stepwise or at constant scanning rate) [10]. Other investigations were done under isothermal conditions and pressure changes were made step-wise or at a constant rate [2,8,11]. The third mode of operation supposes the step-wise, or at a continuous rate, variation of volume under isothermal conditions, with concomitant recording of pressure and heat flux [12]. The possibility of controlling the three most important thermodynamic variables (p, V, and T) in calorimetric measurements makes it possible to perform simultaneous measurements of both thermal and mechanical contributions to the thermodynamic potential changes caused by the perturbation [13]. The simultaneous determination of both thermal and mechanical contributions to the total change of thermodynamic potential not only leads to the complete thermodynamic description of the system under study, but also permits investigation of systems with limited stability or systems with irreversible transitions. This approach is also very useful in analyzing the course of a transition. By a proper external change of the controlling variable, the transition under investigation can be accelerated, impeded, or even stopped at any degree of its advancement and then taken back to the beginning, all with simultaneous recording of the heat and mechanical variable variations. This permits not only determination of the total changes of the thermodynamic functions for the transition but also allows analysis of their evolution along the advancement of the transformation. For this reason the technique was called scanning transitiometry [14]. Nowadays, such *pVT*-calorimeters are currently commercialized (*BGR-Tech Ltd.*, Poland) and one of them was used in this study. The technique has been operated over wide pressure (up to 400 MPa) and temperature (25–300 °C[1]) ranges with the step-wise or the linear scan of the variable change.

One of the aims of this study was to extend the working temperature interval toward low temperatures range (down to −80 °C). When dealing with high-pressure low-temperature calorimetry another challenge must be overcome namely, a suitable combination between the calorimetric block and the cooling device. Advantageously, the calorimetric block, we used in this study, is surrounded by a heating-cooling shield which was connected to a powerful refrigerated heating circulator for closed systems. The first part of present work is devoted to the performances of this assembly.

[1] Although temperature in Kelvin (K) is the recommended thermodynamic temperature, we used for convenience throughout this paper the temperature in Celsius (°C).

The second part is focused on the effect of pressure on the fusion/crystallization of mercury. As it was already mentioned, mercury was often used as pressurizing fluid due to its chemical inertia and very good as well as well-known thermomechanical coefficients ($\alpha_p = 1.80 \times 10^{-4}\,K^{-1}$ and $\kappa_T = 0.41 \times 10^{-4}\,MPa^{-1}$). However, at low temperatures its use it limited, $T_m = -38.83\,°C$, and this temperature increases with pressure. In 1911 Bridgman [15,16], using a high-pressure press, located the melting curve of mercury and thereafter used the equilibrium pressure at 0 °C as a fixed point in the calibration of his manganin-wire resistance gauges, just as the ice point and the boiling point of water at normal atmospheric pressure are used for the calibration of thermometers. His value of the equilibrium pressure, 7492 bars, was obtained by means of a free-piston gauge, and was supposed to be accurate to about 1/10 of 1%. In 1953 Johnson and Newhall [17] described the controlled-clearance piston gauge, or dead-weight tester, which provides a substantial gain in accuracy over the reentrant type developed by Bridgman. In their paper they reported a determination of the mercury 0 °C freezing pressure, stating the value of 7568 bars.

This paper presents the data obtained with scanning transitiometry concerning the effect of pressure, in the pressure range from 0.1 to 100 MPa, on the latent heat of fusion/crystallization of mercury. The experiments were performed in both isobaric scanning temperature and in isothermal scanning pressure conditions. A comparison is made concerning the two modes of operation. The comparison concerns the measured latent heats of fusion/crystallization, the size and shape of recorded heat fluxes, and the delay between the recorded calorimetric and mechanical signals.

2. Experimental part

2.1. Chemicals

Propyl alcohol p.a. with purity >99.5 mole% was provided by (Fine Chemicals) Acros Organics France. It was distilled at atmospheric pressure, under nitrogen atmosphere, prior the use. Mercury was provided by Sigma-Aldrich (99.995%), France, and used without further purification.

2.2. Apparatus

A schematic view of the assembly transitiometer + ultracryostat is shown in Fig. 1. It consists of a *BGR-Tech* scanning transitiometer connected to a *Hüber* unistat, model 390w. The connection between the cryostat and the heating-cooling shield of the calorimetric block is made *via* two flexible thermoisolated hoses.

The transitiometer itself is constructed as a twin calorimeter with a variable volume. It is equipped with high-pressure vessels, a *pVT* system, and LabVIEW-based virtual instrument (VI) software. Two cylindrical calorimetric detectors (Ø = 17 mm, l = 80 mm) each made from 622 thermocouples (chromel-alumel) are mounted differentially and connected to a nanovolt amplifier, which is functioning as a non-inverting

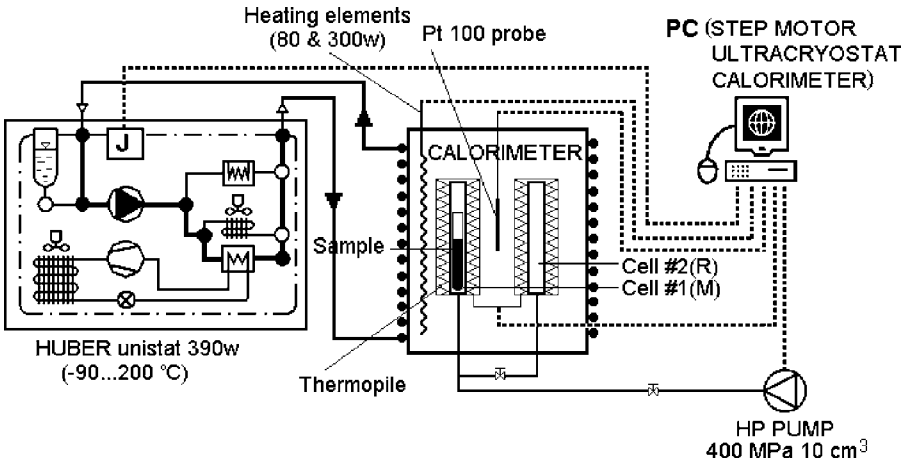

Fig. 1. Schematic view of the assembly scanning transitiometer + cryostat.

amplifier, whose gain is given by an external resistance (with 0.1% precision). The calorimetric detectors are placed in a metallic block, the temperature of which is directly controlled with a digital feedback loop of 22 bits resolution ($\sim 10^{-4}$ °C), being part of the transitiometer software. The calorimetric block is surrounded by a heating-cooling jacket, which is connected to the cryostat. The calorimetric block is embedded by an additional heating-cooling shield. The temperature difference between the block and the heating-cooling shield is set to a constant value (5, 10, 20, or 30 °C) and is controlled by an analogue controller; at low temperature this heating-cooling shield performs only as thermal isolation. The temperature measurements, both absolute and differential, are performed with calibrated 100 Ω Pt sensors. The Pt100 temperature sensor is placed between the sample and the reference cell. The absolute accuracy for isothermal measurements is ±0.05 °C, and in the scanning mode it is ±0.1 °C. The heaters are homogeneously embedded on the outer surfaces of both the calorimetric block and the heating-cooling shield. The whole assembly is placed in thermal insulation enclosed in a stainless steel body and placed on a stand, which permits moving the calorimeter up and down over the calorimetric vessels. When performing measurements near 0 °C or below, dry air is pumped through the apparatus, in order to prevent the condensation of waters vapours from air. A more detailed scheme of the whole assembly is given in Ref. [1]. The variable volume is realized with a stepping motor driven piston pump. The resolution of the volume detection is ca. 5.24×10^{-6} cm^3 per step, as it was found by the measurement of the piston displacement for given numbers of steps. The total variable volume is 9 cm^3. The calorimeter block can be lifted to load the sample into the cell, or for cleaning. The pressure sensors are connected close to the piston pump. Pressure can be detected with a precision of ±4 kPa. When the calorimeter block is lifted the mercury is filled in an open glass ampoule and weighed. Then the ampoule is placed in the sample cell and resting on a spring (in order to be positioned in the central active part of the detector zone), where it is in contact with the hydraulic pressurizing fluid (propyl alcohol). The system is completely filled with alcohol under special attention for the elimination of possible air bubbles, which can affect the accuracy of volume changes during the experiment. After closing the (measuring) cell the calorimeter block is moved down over the two cells which are then located into the cylindrical heat flux detectors.

The cryostat attached to calorimeter was a Huber refrigerated heating circulator for closed systems, unistat 390w model. Its operating temperature ranges from −90 to 200 °C, with temperature stability at −10 °C of 0.02 °C and cooling power at 0, −20, −40, −60 and −80 °C of 5.2, 5, 4.2, 3.1, and 0.9 kW, respectively. The maxim delivery of circulating pump is 40 l/min and the maximal delivery pressure is 1.5 bars. The cryostat is microprocessor controllable and equipped with an RS232 interface. The cryostat is PC-controlled thanks to a *Labwordsoft® 3.01* graphical software. The software allows to build the temperature program (up to 99 sequences), controls the temperature with high accuracy, and performs data acquisition into a file, with a selectable frequency.

2.3. Experimental procedures

As it was already mentioned, fusion/crystallization of mercury under pressure was investigated during both isobaric and isothermal conditions. During isothermal pressure scans the calorimeter temperature is selected firstly, around −40 °C, and the temperature of cooling fluid (cryostat) is programmed to be 20 °C below the calorimeter temperature. In this way the electronic heater control enables an extremely stable temperature during the experiment. The stability of temperature is better than ±1/1000 °C. As soon as the thermal equilibrium is attained, about 2 h, the pressure is adjusted to the desired value. For the investigation of fusion phenomenon the pressure was continuously decreased while for crystallisation it was continuously increased into the pre-established range (e.g. 10–100 MPa). The scanning rates were ranging from 0.2 to 1 MPa min^{-1}, the typical value being 0.4 MPa min^{-1}.

For isobaric temperature scans, the temperature program of calorimetric block was combined with the cryostat program, as illustrated in Fig. 2, in order to assure a stable temperature gradient during temperature scanning experiments; this insures a very stable baseline of the heat flux signal with a minimum of noise. Thus, as Fig. 2(a) shows, during the fusion runs the

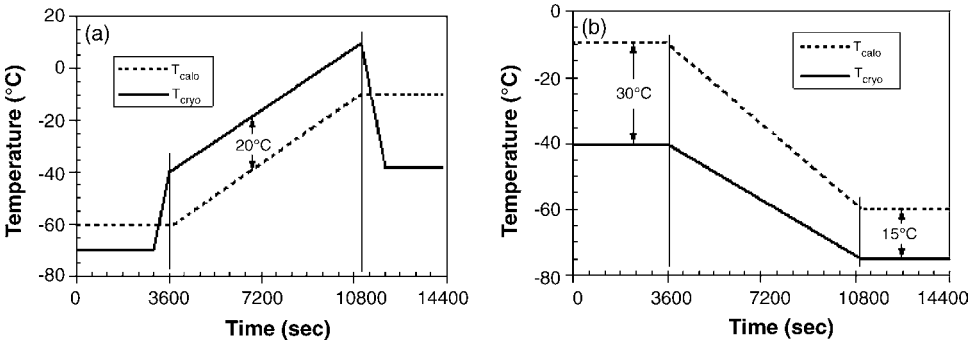

Fig. 2. The temperature program for the transitiometer (dashed line) and cryostat (full line) during isobaric temperatures scans, heating (a) and cooling (b).

temperature of the cooling-heating fluid is lower than that of the calorimetric block during the equilibration periods (isothermal segment) and it is higher, with a gradient of 20 °C, during the dynamic segment; just before the beginning of scanning temperature the temperature of heating/cooling device jumps rapidly (in 5 min) and runs in parallel with the temperature of calorimetric block. In such a way, the scanning rate could be increased to 0.6–0.7 °C min^{-1}, which is about twice the maximal scanning rate with this type of calorimeter but without the help of heating fluid. During crystallisation runs always the temperature of cooling fluid is below the temperature of calorimetric block. However, the initial temperature gradient (e.g. 30 °C) is progressively decreased to 15 °C, because below −80 °C the temperature of cryostat is hardly controlled. Under such conditions, a minimal difference between target and real temperatures and a stable baseline were achieved for scanning rates up to 0.2 °C min^{-1} (typically 0.15 °C min^{-1}).

It is worth notice that the pressure control is achieved with the stepping motor of the high-pressure pump turning only in one direction (compression or decompression) during the experiment. In this way the volume change during the transition is proportional to the recorded number of steps. The data acquisition and process control is enabled with a computer program written in LabVIEW.

2.4. Calibration procedure

The calibration was performed with the melting signal of reference substances, e.g. *n*-octane (−56.76 °C and 180.00 J g^{-1}), *n*-decane (−26.66 °C and 199.87 J g^{-1}), and distilled water (0.01 °C and 333.5 J g^{-1}). The calorimetric peaks were recorded and their integration allowed to calculate the sensibility coefficient of calorimeter which depends by the gain of nanovolt amplifier. The average value of three determinations was considered.

3. Results and discussion

3.1. Validation of the pVT-calorimeter + ultracryostat assembly

As it was already mentioned, performing high-pressure low-temperature *pVT*-calorimetry is a challenge and a special attention should be paid to the proper functioning of the whole experimental set-up. It is well-known that calorimetric block of a Calvet-type calorimeter is rather bulky with high thermal inertia and large time constant. Consequently, a powerful freezing unit is required to bring the calorimetrer at low temperatures (below −70 °C). On the other hand Calvet-type calorimeters are highly sensitive instruments and any perturbation of the temperature of calorimetric block is reflected in the stability of baseline and induces a noisy heat flux signal. This means that in addition to a powerful and easy programmable cryostat, a heating-cooling fluid with excellent physical properties at low temperature (e.g. viscosity, thermal stability, heat capacity, etc.) is required. The most complex temperature program is that used during isobaric runs with positive slope of temperature (mercury fusion) and the recorded temperatures for both cryostat (heating-cooling fluid) and calorimetric block (sample) are illustrated in Fig. 3.

Evidently, the heating-cooling fluid temperature fits reasonably well the programmed temperature with the exception of the parts were sudden changes of temperature slope occur. As is seen in the upper part of Fig. 3(a) the worst situation happens at the end of temperature jump from −70 to −40 °C and at the beginning of temperature increase with slope equal to the calorimeter scanning rate, i.e. 0.4 °C min^{-1}. In other words, the temperature signal corresponding to the heating fluid is noisy in the first half of hour from the beginning of dynamic segment of calorimeter program of temperature. This behaviour induces a deflection of the real temperature of calorimeter to target temperature of about 0.8 °C which exponentially diminishes and fits well with the target temperature in about 45 min. Consequently, in this mode of operation the initial temperature should be about 20 °C below the expected transition temperature. Of course, a simple three temperature segments program of the cryostat, keeping all the time the cryostat's temperature below the calorimetric block's temperature with constant gradient of temperature gives better results. The first mode was privileged because another goal was to investigate the pressure effect on a polymer glass transition, and it is recognized that the associated heat effect to this transition is weak; it increases with increasing the scanning rate. With this mode of operation, just at the beginning of dynamic segment of temperature, the cooling fluid becomes a heating fluid for the calorimetric block and working together with the heating element allows higher scanning rates.

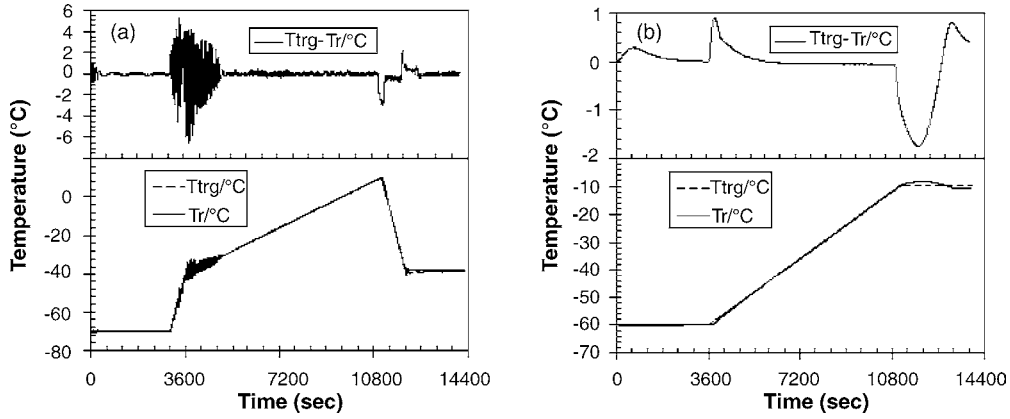

Fig. 3. Temperature evolution during the experiment for the cryostat (a) and calorimetric block (b). In the upper part the differences between the target temperatures and the real ones are given in both cases. Scanning temperature rate, 0.4 °C min^{-1}; pressure, 50 MPa.

An additional advantage of working with a constant gradient of temperature between the colorimeter and cryostat is illustrated in Fig. 4. Since the temperature gradient between the "heating fluid" and the calorimetric block was kept constant (20 °C) the power uptake of the heating elements was quasi-constant, around 40% of total power with the exception of beginning of the dynamic segment, so that the interference of sudden changes of power uptake on the calorimetric signal was avoided.

3.2. Temperature calibration

For temperature calibration, the fusion temperatures of mercury and water at atmospheric pressure have been taken as reference. The choice of these substances is justified by the fact that the measured transition temperatures in the present work range between the transition temperatures at normal pressure of the two references. In accordance with IST-90, the recommended fusion temperatures are 234.3156 K (−38.8344 °C) and 276.16 (0.01 °C) for mercury and water, respectively; from NIST reports, the corresponding recommended enthalpies of fusion are, in order, 11.469 ± 0.008 J g^{-1} and 333.5 ± 0.2 J g^{-1}, respectively [18–20]. The average values of four measurements for fusion temperatures at normal pressure were −37.5159 ± 0.0325 °C for mercury and 0.1235 ± 0.0319 °C for water. The deviation between the measured and calibration temperatures increases from 0.1135 to 1.3185 °C when the temperature decreases from 0 to about −39 °C. To calculate the corrected temperature T_{corr} from the measured temperature T_{meas} we used the following linear regression equation:

$$T_{corr} = 1.032014T_{meas} - 0.117454 \quad (1)$$

with the temperature in °C. As usual, the transition temperature was determined from the extrapolated onset of phase transition. The overall uncertainty of corrected temperatures was below 0.065 °C. The temperature sensor being placed in the calorimetric block and not in contact with the pressurised sample (see Fig. 1), we assumed that the pressure does not affect the accuracy of temperature measurement and the Eq. (1) was further used to make the temperature correction in all experiments carried out under pressure.

3.3. Isobaric fusion/crystallization of mercury

A typical example of mercury fusion at 50 MPa during temperature scanning at 0.4 °C min^{-1} is given in Fig. 5. The scanned interval of temperature was between −60 and −10 °C. The four recorded variables, pressure, temperature, calorimetric signal, and associated volume change, are plotted against time.

The pressure p was kept constant by controlling the volume change V of the high pressure, HP, line. The pressure deviation

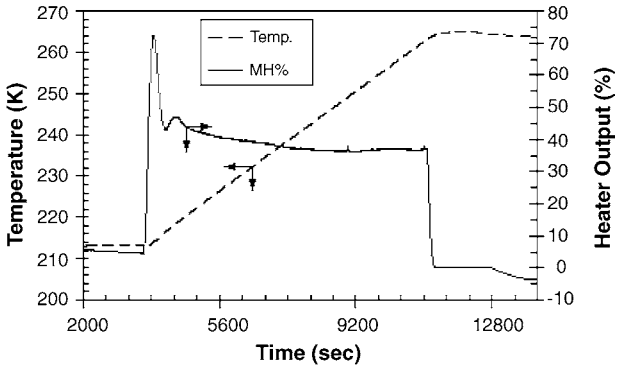

Fig. 4. Evolution of the calorimetric bock temperature and heater uptake (% of total power) during a temperature scan, 0.4 °C min^{-1}, under isobaric conditions.

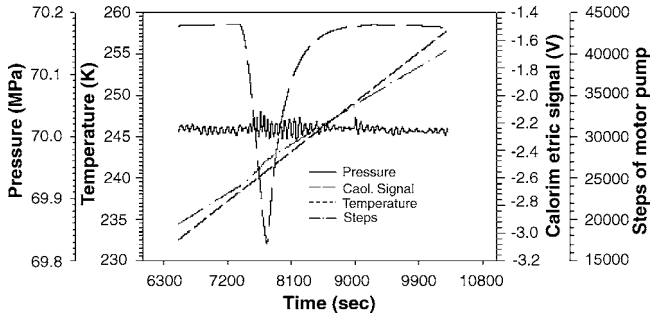

Fig. 5. Illustration of the raw data recorded during the isobaric temperature scanning between −60 and −10 °C. The scanning rate, pressure, and sample mass were 0.4 °C min^{-1}, 50 MPa and 5.569 g, respectively.

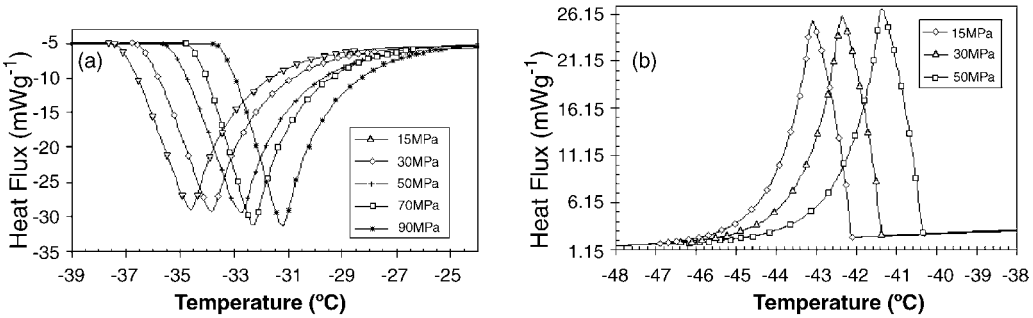

Fig. 6. Thermograms of mercury fusion (a) and crystallization (b) at different pressures. The scanning temperature rates were 0.4 and −0.15 °C min^{-1}, respectively.

Table 1
Pressure dependence of the mercury fusion temperature (in °C) and enthalpy of fusion

Pressure (MPa)	T_{onset} (°C)	T_{peak} (°C)	T_{offset} (°C)	Peak height A_i (mW g^{-1})	Peak width at half-height W_i (°C)	$\Delta_{fus}H$ (J g^{-1})
15	−38.285	−35.878	−33.602	−24.868	2.469	11.456
30	−37.389	−35.054	−32.783	−24.986	2.419	11.466
50	−36.366	−34.074	−31.876	−25.331	2.453	11.470
70	−35.536	−34.473	−31.017	−26.198	2.181	11.483
90	−34.412	−32.357	−30.356	−26.854	2.221	11.498

from the target value was ±0.03 MPa, with little noise around the phase transition. When the temperature reached the corresponding phase change temperature, the sample started melting. The peak increased until the complete melting of the sample and declined back to the initial base line. A significant volume change is also seen at the melting transition.

The pressure effect on the melting of mercury is illustrated by five calorimetric plots obtained at 15, 30, 50, 70, and 90 MPa in Fig. 6(a) and on its crystallization is illustrated by three calorimetric plots at 15, 30, and 50 MPa, Fig. 6(b), respectively.

As can be seen in Fig. 6(a) both the fusion temperature, T_{fus}, and the solidification temperature, T_{cr}, are shifted toward higher temperatures with increasing the pressure. In Fig. 6(a) the fusion peaks obtained at 70 and 90 MPa seem to be more intense, but this is related to the fact that the gain of nanovolt amplifier was increased from 1501 to 3401 for the two experiments. The heat flux curves were defined by the following parameters: peak height, A_i, peak width at half-height, W_i, and peak position, T_{tr} or p_{tr}, depending on the experimental conditions, i.e. isothermal or isobaric measurement. On its turn, the peak position was always determined from the intercept of the greatest slopes of the calorimetric curve with the baseline, as T_{onset} or T_{offset}, and T_{peak} as the temperature corresponding to the intersection of the two tangents. The fusion heat was evaluated by integrating the calorimetric peak corrected by the sensibility coefficient, after subtraction of the baseline. The data concerning the effect of pressure on the mercury fusion are collected in Table 1. The enthalpy of fusion is almost the same (slightly increasing with pressure). As this table shows the larger intensities of the peaks recorded at 70 and 90 MPa are compensated by lower peaks width at half-height W_i.

The volume changes associated to the mercury fusion/crystallization were simultaneously recorded and are plotted in Fig. 7(a). The derivatives of volume change with temperature are also illustrated in Fig. 7(b), after smoothing.

There is a good accordance between the effect of pressure on the transition temperatures measured by enthalpy of fusion and volume change, Table 2. The variation of fusion temperature with pressure was also calculated from the peaks of rate of volume change variation with temperature. In addition, the volume change was calculated *via* Clausius-Clapeyron equation, Eq. (2), and the obtained results are compared with

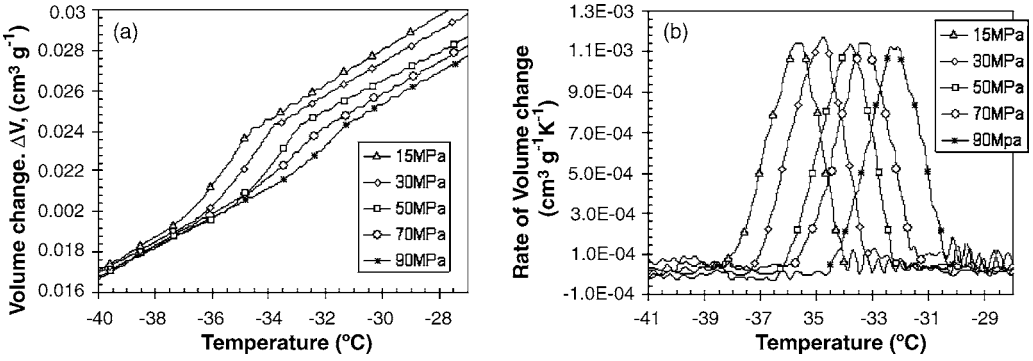

Fig. 7. Specific volume variation, ΔV_{spec}, as a function of temperature and pressure (a) and the rate of volume change, $d(\Delta V_{spec})/dT$, (b) during the mercury fusion under isobaric conditions.

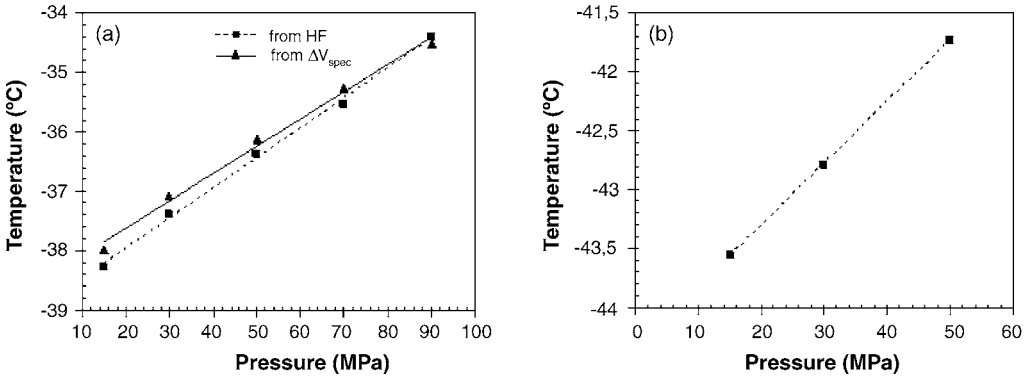

Fig. 8. Pressure dependence of the mercury fusion (a) and crystallization (b) temperatures. The temperature scanning rates were 0.4 and −0.15 °C min^{-1} for fusion and crystallization experiments, respectively. In (a) results from specific volume change measurements together with the regression curve (full line) are also given.

Table 2
Comparative fusion temperatures and volume changes obtained from calorimetric and *pVT* measurements, and from *pVT* measurements *via* Clausius-Clapeyron equation during mercury fusion at different pressures

Pressure (MPa)	T_{onset} (°C) from:		$\Delta_{fus}V_{spec}$ (10^{-3} cm^3 g^{-1})	
	Heat flux	$d(\Delta V_{spec})/dT$	Experimental	Calculated from Eq. (2)
15	−38.285	−37.987	2.491	2.497
30	−37.389	−37.086	2.451	2.450
50	−36.366	−36.117	2.423	2.441
70	−35.536	−35.262	2.411	2.439
90	−34.412	−34.503	2.398	2.426

the experimental ones.

$$\frac{dT_{tr}}{dp} = \frac{\Delta_{tr}V}{\Delta_{tr}S} = T_{tr}\frac{\Delta_{tr}V}{\Delta_{tr}H} \quad (2)$$

As Table 2 and Fig. 8(a) show the fusion temperatures determined from volume change measurements are slightly shifted toward higher temperatures and the temperature difference continuously decreases, from 0.3 to 0.1 °C with the increase of pressure from 15 to 90 MPa. In addition, the calculated volume changes during transition *via* Eq. (2) are higher then the experimentally obtained by integration of the peaks depicted in Fig. 7(b), especially at high pressure (over 50 MPa). The difference comes from both integration accuracy of the $d(\Delta V_{spec})/dT$ curves, which are noisy and suffered severe smoothing, and from fusion temperature values, which were taken from mechanical (volume changes) curves.

The representation of fusion and crystallization temperatures as functions of pressure give the plots represented in Fig. 8(a) and (b). From these values as well from the data collected in Tables 1 and 2 the following regression curves have been calculated:

$$T_{fus} = T_0 \pm 0.2921 + (0.0504 \pm 0.00506)p \quad (3)$$

$$T_{crist} = -44.340 \pm 0.127 + (0.052 \pm 0.00366)p \quad (4)$$

$$\Delta_{fus}V = \Delta_{fus}V_0 \pm 1 \times 10^{-4} - (2.894 \pm 0.477)10^{-6}p + (1.643 \pm 0.445)10^{-8}p^2 \quad (5)$$

where p is the pressure in MPa, $T_0 = -38.8344$ °C (from IST-90 [20]) and $\Delta V_0 = 2.467 \times 10^{-3}$ cm^3 g^{-1} (from $\Delta_{fus}H_0 = 11.469$ J g^{-1} *via* the Clausius-Clapeyron equation) are chosen so as to fit the well-known best values of this substance at normal pressure. In Eqs. (3) and (4) the given standard deviation define the limits of best value estimation and leads to an uncertainty of about 0.5 and less than 0.4 °C at 100 MPa for fusion and crystallization temperatures, respectively.

In Eqs. (3) and (4) the two slopes $dT_{fus}/dp = (0.0504 \pm 0.00506)$ and $dT_{crist}/dp = (0.052 \pm 0.00366)$ are close enough to each other and relatively small, which suggest a small effect of pressure on the mercury transition temperatures.

The pressure dependence of the heat of fusion of mercury may be estimated from the heat flux data as:

$$\Delta_{fus}H = \Delta_{fus}H_0 - (3 \pm 2.2)10^{-4}p + (7.529 \pm 2.342)10^{-6}p^2 \quad (6)$$

where p is the pressure in MPa and $\Delta_{fus}H_0 = 11.469 \pm 0.008$ J g^{-1} at normal pressure. The enthalpy of fusion increases somewhat with pressure; this increase is less than 0.5% per 100 MPa in the investigated range of pressure.

3.4. Isothermal fusion/crystallization of mercury

It is recognized that the pressure scanning has an opposite effect to the temperature scanning on the fusion/crystallization; thus the melting occurs during the increase of temperature and during pressure decrease (decompression) while the solidification occurs during temperature decrease and pressure increase (compression) under isothermal or isobaric conditions, respectively. Consequently, the fusion of mercury was investigated during pressure scanning from 100 to 1 MPa at a constant rate, typically 0.4 MPa min^{-1}. The raw data acquired at −39 °C are plotted in Fig. 9. As depicted in this figure, when the pressure decreases to reach the corresponding phase change temperature (calorimeter's temperature) the sample starts melting and the associated volume change suddenly modifies the slope. The peak of fusion increases almost linearly until complete melting of mercury and declines back quickly to the baseline.

Table 3
The main characteristics of mercury fusion peaks obtained during isothermal pressure scans (decompression)

T_{fus} (°C)		p_{onset} (MPa)	Peak height, A_i (mW g^{-1})	Peak width at half-height W_i (MPa)	$\Delta_{fus}H$ (J g^{-1})
T_{meas}	T_{corr}				
−39.0	−40.366	28.592	8.104	9.014	11.359
−38.5	−39.850	37.682	8.037	9.175	11.336
−38.0	−39.334	47.065	10.196	7.571	11.543
−37.5	−38.818	56.120	10.096	7.509	11.448
−36.5	−37.786	74.993	9.829	8.036	11.502

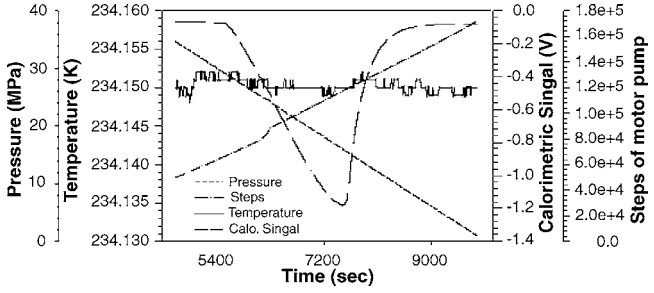

Fig. 9. Illustration of the raw data recorded during the isothermal pressure scanning between 100 and 1 MPa. The scanning rate, temperature, and sample mass were 0.4 MPa min^{-1}, −39 °C and 5.569 g, respectively.

Six calorimetric plots at temperatures ranging from −39.5 to −36.5 °C with a temperature step of 0.5 °C are presented in Fig. 10(a). The solidification of mercury happens during pressure increase and three calorimetric plots illustrating this process at −40, −39.5, and −39 °C are given in Fig. 10(b). The pressures corresponding to the phase change increase with increasing the temperature. The main characteristics of the fusion peaks are given in Table 3.

Once again, the heats of fusion evaluated by integrating the calorimetric peaks are in fairly good accordance with the data from literature (refs. [18] and [20]) even better than those obtained during isobaric conditions. The peaks are less regular as those obtained under isobaric condition, but the differences in peaks heights, A_i, are compensated by peaks width at half-height, W_i, which led to almost the same values of enthalpy of fusion. In addition, the melting pressures were experimentally repeatable but the freezing pressures were not, that is the amount of superpression varies erratically.

The temperature dependence of the pressures corresponding to the onset of melting gives a straight line, Fig. 11, with the

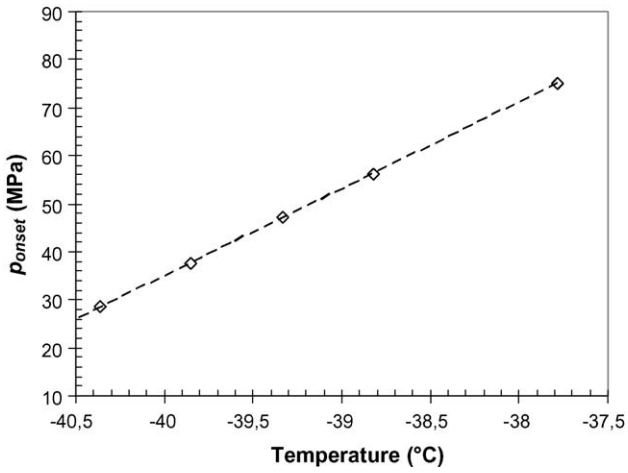

Fig. 11. Temperature dependence of the pressure corresponding to the beginning of mercury fusion (together with the regression curve). The pressure scanning rate was 0.4 MPa min^{-1}.

regression Eq. (7):

$$p_{fus} = (18.0154 \pm 0.366)T + 755.6 \pm 14.497 \quad (7)$$

where T is the working temperature in °C. Extrapolation to the ordinate gives the value of 755.6 MPa which is in good agreement with the value found by Johnson and Newhall, 756.8 MPa, for the mercury at 0 °C freezing pressure.

The impact of the pressurization rate appears clearly in Fig. 12 and Table 4. As Fig. 12(a) shows, when represented in function of time, the peaks height increases and becomes narrower with increasing pressurization rates. However, when the heat flux (peak height) is plotted against pressure (Table 4) it is evident that as for isobaric calorimetry, a higher scanning rate yields a lager span of the peak. Thus, the span, expressed by the peak

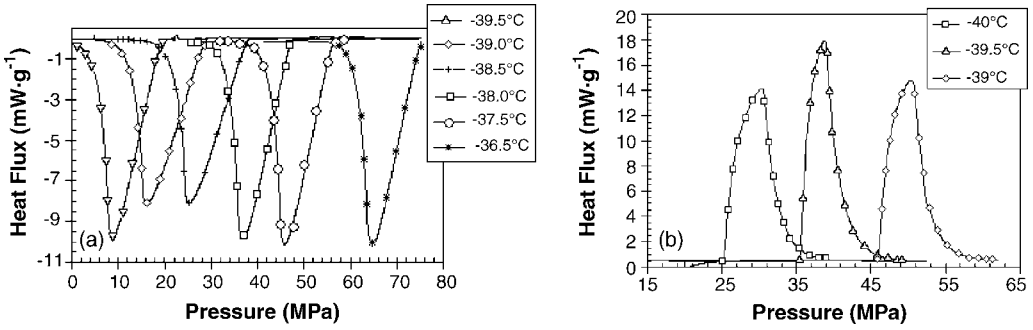

Fig. 10. Thermograms of mercury fusion (a) and crystallization (b) at different temperatures. In both cases the scanning pressure rate was 0.4 MPa min^{-1}.

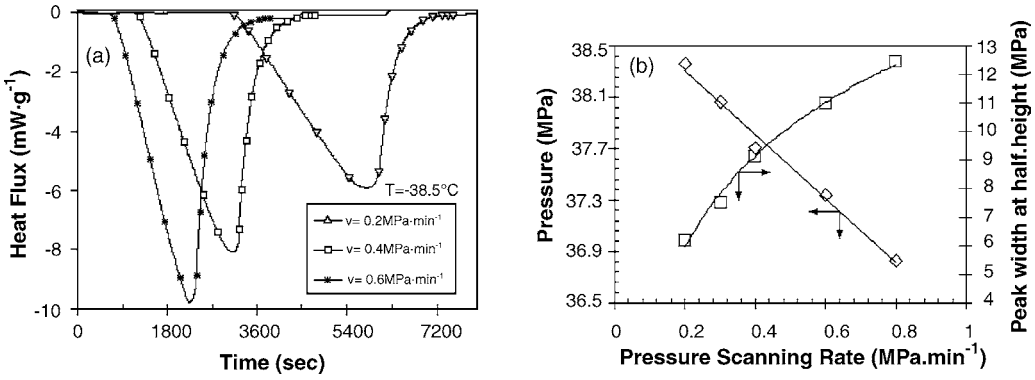

Fig. 12. Thermograms of mercury fusion in function of pressure scanning rate (a) and the scanning rate effect on the pressure corresponding to the onset of mercury fusion and peak width at half-height (b).

Table 4
Effect of pressure scanning rate on the main characteristics of the fusion peaks

Scanning rate (MPa min^{-1})	p_{onset} (MPa)	p_{peak} (MPa)	p_{offset} (MPa)	Peak height, A_i (mW g^{-1})	Peak width at half-height W_i (MPa)
0.2	38.364	29.187	27.71	5.896	6.188
0.3	38.069	26.864	25.031	7.055	7.524
0.4	37.704	24.826	22.961	8.067	9.131
0.6	37.336	21.967	18.323	9.705	10.982
0.8	36.828	20.371	14.801	11.516	12.479

width at half-height, increases from 6.18 to 12.48 MPa when the scanning rate increases from 0.2 to 1 MPa min^{-1}.

As it is seen in Fig. 12(b), at a given temperature the fusion pressure decreases with increasing the pressurizing rate. Applying a regression function to our mercury data gives:

$$p_{fus} = (-2.2255 \pm 0.481)\frac{dp}{dt} + 38.63 \pm 0.244 \quad (8)$$

where dp/dt is the pressure scanning rate in MPa min^{-1} and p_{fus} is the pressure (in MPa) corresponding to the beginning of mercury fusion at a given temperature ($T_{meas} = -38.5\,^{\circ}C$). The p_{fus} is shifted toward lower values by about 2.23 MPa when the pressure scanning rate increases with 1 MPa min^{-1}.

3.5. Comments concerning temperature versus pressure scanning

In Fig. 13 typical thermograms of mercury fusion/solidification from temperature scanning (0.4 °C min^{-1} at 50 MPa) and pressure scanning (0.4 MPa min^{-1} at −39 °C) are depicted. In both cases the heights of crystallization peaks are higher compared to that of fusion peaks which, in turn, are more spanned. As Fig. 13(a) shows, at the same pressure, the crystallization starts at lower temperatures, the supercooling shift being of about 5 °C; the same behaviour was observed under isothermal conditions, where the superpression is of about 18 MPa.

At studied scanning rates, the heights of the melting/solidification peaks are higher under isobaric conditions, almost twice in the case of crystallization and three times higher for melting curves, which is more clearly depicted in Fig. 14(a), where an additional coordinate axis was added for sake of clarity. According to the data given in Table 4 concerning the effect of the pressure scanning rate on the peaks height and width at half-height and the analysis of the equations describing their evolution with scanning rate suggests that a pressure scanning rate of more than 2 MPa min^{-1} is required in order to have heat flux curves with comparable

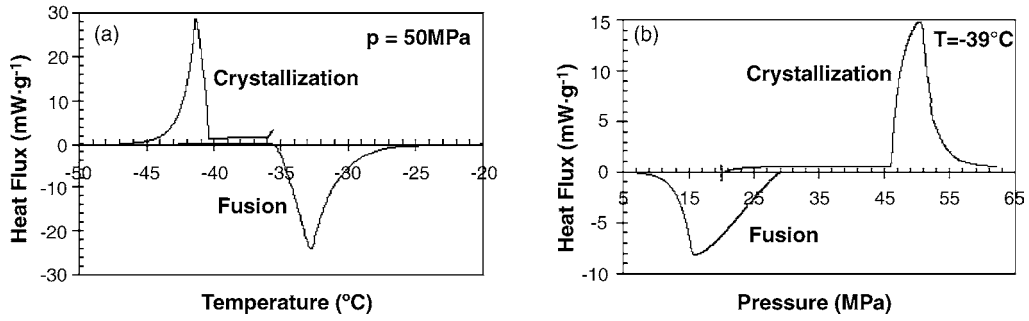

Fig. 13. Heat flux curves obtained during isobaric temperature scanning (a) and isothermal pressure scanning (b). The positive heat flux curves correspond to crystallization (descending temperature and ascending pressure), while those below 0 heat flow correspond to melting (ascending temperature and descending pressure).

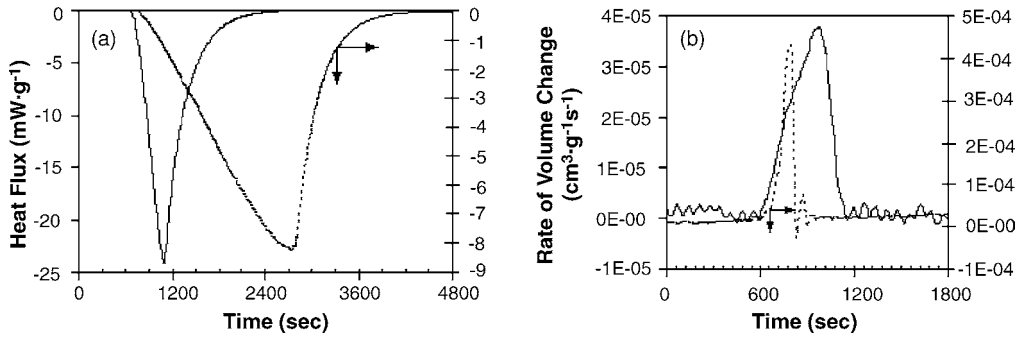

Fig. 14. Heat flux curves (a) the rates of volume change, $d(\Delta V_{spec})/dt$, (b) obtained during isobaric (full line) and isothermal (dashed line) conditions. The conditions of measurements were those given in Fig. 12.

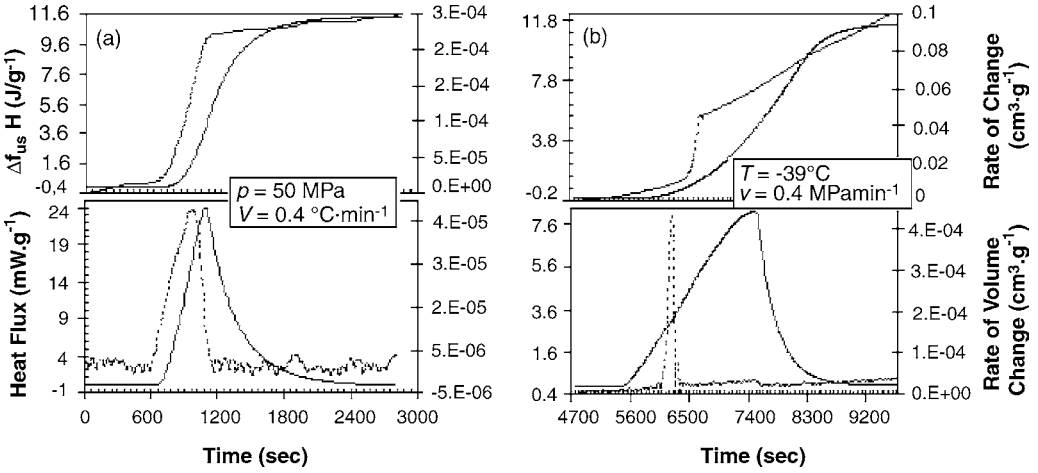

Fig. 15. Heat flux curves and their integrals (enthalpies) (full lines) of the mercury fusion and associated volume changes and their derivatives, $d(\Delta V)/dt$ (dashed lines) obtained under isobaric (a) and isothermal (b) conditions.

height and span to those obtained during temperature scanning.

Unexpectedly, when the rates of volume change are considered, Fig. 14(b), the peak corresponding to the pressure scanning is narrower and its intensity is higher with almost one order of magnitude than the corresponding one to the temperature scanning under isobaric conditions. In order to clarify this aspect, in Fig. 15 both the heat fluxes and their integrals (enthalpies) and the volume changes and their derivatives $d(\Delta V_{spec})/dt$ are plotted against time for isothermal and isobaric measurements. For sake of simplicity the melting heat fluxes and their integrals were taken in absolute value. As expected, during temperature scanning, Fig. 15(a), the phase change is firstly distinguished by the volume change, most likely due to the high time constant of the calorimeter. In the ascending part of the heat flux and rate of volume change curves, the two signals runs almost parallel but the derivative of volume change declines back faster. During pressure scanning, Fig. 15(b), apparently the fusion is firstly distinguished from calorimetric measurement but, after a while, the volume variation associated to the melting suddenly changes of slope and the whole transition takes less than 4 min whereas from calorimetric measurement the phase change requires about 1 h. This peculiar behaviour is still under investigation.

4. Conclusions

In our work a *pVT*-Calvet type differential calorimeter was coupled with a powerful cryostat in order to investigate the effect of pressure on the phase transitions and corresponding transition temperatures at low temperatures (up to −80 °C). Both devices are PC controlled, allowing independent programming of temperature sequences, temperature control during experiment, and data acquisition for offline analysis of assembly performances. In the first part, a careful analysis of recorded temperatures of the calorimetric block and of the heating/cooling fluid and their deviation from the target temperatures allowed the validation of both assembly and chosen experimental technique.

In the second part, mercury phase transitions under pressure were investigated by scanning transitiometry in the pressure range from 0.1 to 100 MPa. Mercury was selected as model substance due to the fact that it is widely used as pressurizing fluid in high-pressure calorimetric measurements. Reproducible measurements were obtained with this set-up and the resulting phase transition parameters are in good agreement with literature values. The experiments were performed both under isobaric conditions (temperature scanning) and isothermal conditions

(pressure scanning) and the most relevant findings lead to the following conclusions.

Both in isothermal and isobaric conditions the latent heat (enthalpy) of fusion of mercury, obtained by integration of heat flux curves, was in good agreement with literature values ($11.469 \pm 0.008\,\mathrm{J\,mol^{-1}}$ at normal pressure), slightly increasing with pressure (the increase is less than 0.5% per 100 MPa) in the investigated range of pressure.

- Under isobaric conditions both the fusion and crystallization temperatures increase linearly with pressure; the two slopes $\mathrm{d}T_{\mathrm{fus}}/\mathrm{d}p$ and $\mathrm{d}T_{\mathrm{crist}}/\mathrm{d}p$ were 0.0504 ± 0.00506 and $0.052 \pm 0.00366\,^{\circ}\mathrm{C\,MPa^{-1}}$, respectively.
- Under isothermal conditions the pressures corresponding to the phase transitions also increase linearly with increasing the temperature, with a slope of $18.0154 \pm 0.366\,\mathrm{MPa\,^{\circ}C^{-1}}$. Further, the extrapolation of the fitting equation $p_{\mathrm{m}} = f(T)$ at 0 °C freezing pressure gives the value of 755.6 ± 14.497 MPa that in accordance with literature value (756.8 MPa in ref. [17]).
- The pressure scanning rate affects the shape of the calorimetric curves; thus, both the height of heat flux curves and the pressure span, expressed by peaks width at half-height, increase with scanning rate. As compared to heat flux curves obtained under isobaric conditions the heat flux curves recorded during pressure scanning are less intense and more spanned and pressure scanning rates of more that $2\,\mathrm{MPa\,min^{-1}}$ are required in order to have similar curves.
- Due to the supercooling and superpression effects the solidification is retarded with respect to melting by about 5 °C and 18 MPa under isobaric and isothermal conditions, respectively.

The main advantage of *pVT*-calorimetry is the possibility of concomitant recording of both the heat flux and the volume variations associated to the phase transition. The measured volume changes are accurate and in good accordance with the values calculated *via* Clapeyron equation from experimental heats of fusion. The data furnished by the two techniques are complementary to each other and their critical analysis allows a more accurate interpretation of the phase transition phenomenon. Thus, due to the large time constant of calorimeter the calorimetric phase transitions are a little delayed and spanned as compared to those obtained from volumetric measurements.

Acknowledgements

The authors, and especially F. Dan, are grateful to the French National Council of Scientific Research (CNRS-France) for its support through an associate researcher position. Thanks are due also to Miss. M. Chabut for her help in performing calorimetric measurements.

References

[1] J.-P.E. Grolier, F. Dan, S.A.E. Boyer, M. Orlowska, S.L. Randzio, Int. J. Thermophys. 25 (2) (2004) 297–319.
[2] G.W.H. Höhne, Thermochim. Acta 332 (1999) 115–123.
[3] A. Le Bail, D. Chevalier, J.M. Chourot, J.Y. Monteau, J. Therm. Anal. Cal. 66 (2001) 243–253.
[4] J.C. Petit, K.L. TerMinassian, J. Chem. Thermodyn. 6 (1974) 1139–1152.
[5] S.L. Randzio, J.-P.E. Grolier, J.R. Quint, Rev. Sci. Instrum. 65 (1994) 960–965.
[6] J.M. Chourot, A. LeBail, D. Chevalier, High Pressure Res. 19 (2000) 191.
[7] S.L. Randzio, Ch. Stachowiak, J.-P.E. Grolier, J. Chem. Thermodyn. 35 (2003) 639–648.
[8] K. Fischer, M. Wilkem, J. Gmehling, Fluid Phase Equilib. 210 (2003) 199–214.
[9] S.A.E. Boyer, S.L. Randzio, J.-P.E. Grolier, J. Polym. Sci.: Polym. Phys. 44 (2006) 185–194.
[10] S.L. Randzio, J. Therm. Anal. Cal. 57 (1999) 165–170.
[11] S.L. Randzio, Thermochim. Acta 330 (1997) 29–41.
[12] S.A.E. Boyer, M.-H. Klopffer, J. Martin, J.-P.E. Grolier, J. Appl. Polym. Sci., in press.
[13] S.L. Randzio, Pure Appl. Chem. 63 (1991) 1409–1414.
[14] S.L. Randzio, Chem. Soc. Rev. 25 (1996) 383–392.
[15] P.W. Bridgman, Proc. Am. Acad. Arts Sci. 47 (11) (1912) 321.
[16] P.W. Bridgman, Proc. Am. Acad. Arts Sci. 47 (12) (1912) 388.
[17] D.P. Johnson, D.H. Newhall, Trans. Amer. Soc. Mech. Engrs. 75 (1953) 301.
[18] S. Stølen, F. Grønvold, Thermochim. Acta 327 (1999) 1–32.
[19] N.S. Osborne, J. Res. Natl. Bur. Stand. 23 (1939) 643–646.
[20] J.E. Callanan, K.M. McDermott, E.F. Westrum, J. Chem. Thermodyn. 22 (1990) 225–230.